EFFECTS OF COPPER OXIDE AND SULFURIC ACID ON THE PYROLYSIS BEHAVIOR OF AMMONIUM NITRATE UNDER THERMAL RADIATION EXPERIMENTS

[1]Asadjon Qambarov, [2]Tursunoy Navruzova, [3]Mukhlisa Davlatmirzaeva, [4]Iskandar To‘raboyev, [5]Zarifjon Salimov

[1,2,3,4,5] Yangiyer branch of Tashkent Institute of Chemical Technology

https://doi.org/10.5281/zenodo.7979264

Abstract. *Statistics have indicated that industrial accidents of ammonium nitrate were primarily caused by uncontrolled external fires where heating was dominantly controlled by radiation, and yet existing studies at milligram scale cannot fully simulate the real fire scenarios. To explore the pyrolysis behavior in typical fires, this study conducted thermal radiation experiments using pure ammonium nitrate, and its mixtures with copper oxide and sulfuric acid. Different from the pyrolysis process identified in milligram scale tests, the bench-scale pyrolysis of ammonium nitrate under radiation consisted of four stages. Pyrolysis structure model of each stage was built to reveal the differences in dominated thermal behavior. Results indicated that two additives had different thermochemical effects on pyrolysis of ammonium nitrate. Sulfuric acid accelerated the reaction rate of each stage by generating catalytic nitric acid; copper oxide reduced the number of reaction stages into three via surface absorptions. The time and mass loss rate of different stages were determined. Recommendations on effective emergency response were made to prevent the transition of slow decomposition into fast decomposition, and thus to intervene the fire-induced domino effect of ammonium nitrate. This study helps to understand the pyrolysis behavior of ammonium nitrate under fire exposure, and provides insights for pyrolysis modeling and firefighting in industry of interest.*

Keywords: *ammonium nitrate, thermal radiation, mass loss rate, pyrolysis behavior, emergency response.*

INTRODUCTION

Ammonium nitrate (AN) is one of the most widely known hazardous chemicals. It is generally used as the nutrient in agricultural fertilizers and the oxidizer in explosives [1,2] for the advantages compared with other oxidizers, including low cost, easy availability, strong gas generation, chlorine free combustion nature and so on [3]. As an important green oxidizer [4] and a commonly used commercial product, AN is playing an increasingly important role in the development of ecofriendly solid fuels. However, the inherent thermal instability of AN often leads to fire and explosion accidents during storage and transport. A number of studies related to hazards of AN and mixtures under elevated temperature have been published. According to Marlair and Kordek [5], the thermal hazards of AN are threefold, including fire hazard, thermal decomposition hazard, and explosion hazard. One major safety problem of AN is that it melts and decomposes when heated over 170 °C. Studying the thermal stability of AN and effects of additives has been a popular topic for many years [6]. Recently, Babrauskas and Leggett [1] published so far the most extensive and complete review related to thermal hazards of AN. According to the review, applying thermal analysis techniques (e.g. TGA, DSC, C80) to study the decomposition of milligram AN substances in inert or oxidizing atmosphere, and at various heating

rates, has become a fundamental procedure. Through a series of data processing, thermal runaway hazards of AN were generally described by onset decomposition temperature, heat of reaction, activation energy, pressure release rate, mass loss and so on [6–14]. It is widely accepted that AN has a single pyrolysis stage under elevated temperature. However, AN related thermal behaviors are much complicated in real fire accidents. Oxley et al. [8] summarized seven typical patterns including, blast → explode, fire → explode, fire no explode, thermal runaway → fire → no explode, thermal runaway → detonation, fire → blast → detonation and blast no detonation. Similarly, Babrauskas [15] reviewed the AN related explosions throughout a century and found that 100% of AN's explosion accidents in storage or transport had a single causative factor, the uncontrolled external fire. For instance, the catastrophic fire and explosion accidents that occurred at Tianjin Port, China in 2015 [16,17] followed this pattern.

Nomenclature

MLR (g s^{-1}) Mass Loss Rate
MLR_I (g s^{-1}) Mass Loss Rate at the end of stage I
MLR_{II} (g s^{-1}) Mass Loss Rate at the end of stage II
MLR_{max} (g s^{-1}) Mass Loss Rate at the end of stage III (the maximummass loss rate)
t_I (s) Time at the end of stage I
t_{II} (s) Time at the end of stage II
t_{max} (s) Time at the end of stage III (time at the maximum mass loss rate)
t_{end} (s) Time at the end of stage IV (total time of pyrolysis process)ISO International Standardization Organization

AN	Ammonium Nitrate
CuO	Copper OxideH_2SO_4 Sulfuric Acid
C80	C80 Micro Calorimeter
DSC	Differential Scanning Calorimetry TG Thermogravimetry
XRD	X-Ray Diffraction
IR	Infrared Radiation
SEM	Scanning Electron MicroscopeR Reaction
l	Liquid
s	Solid
g	Gas

The initial fire was caused by the self-ignition of nitrocellulose, and yet the large amount of AN acting as both explosives and strong oxidizers strongly supported the evolution of fire and caused pronounced fires and explosions, killing 165 people. The role of AN here is a typical fire-induced domino effect, which combines an uncertain event (the primary fire accident of nitrocellulose) and deterministic events (the secondary fire and explosion accidents of AN) [18]. As a low-frequency high consequence chain of accidents, the primary threat of domino effect is that the consequences of secondary accidents are much more severer than the consequence of the primary accident [19,20]. The Tianjin Port accident has drawn high attention from researchers to consider adopting new methodologies and perspectives to study the thermal behavior of hazardous chemicals [21]. Existing findings through milligram scale experiments may not provide sufficient information to describe the thermal process of AN and mixtures in real fire, or to support emergency responses in industrial accidents. Babrauskas and Leggett's review [1] also highlighted that, most of the explosions of AN involved fire as the proximate cause, and yet there are limited

studies that heating AN by fire radiation or to explore the firefighting of AN in fire. A relevant work by Han et al. [22] studied the capability and complications when using water to extinguish fires involving AN stock, and proposed the mechanism for thermal decomposition developing to detonation. As one of the few articles, this paper emphasized that AN fire is a thermal process that differs from normal combustions due to the complicated physical and chemical characteristics [22]. The chemical mechanism during decomposition of AN in milligram scale has been widely discussed, and yet limited studies analyze the chemicals in bench scale with fire radiation dominated heating. This paper applies a Desktop Cone Heating Apparatus (DCHA) to simulate the fire radiation-controlled heating scenario, and measures the mass loss rate (MLR) to characterize the pyrolysis behavior of AN and mixtures exposed to radiation in different intensities. Among varied additives, two catalysts, copper oxide (CuO) and sulfuric acid (H_2SO_4) are selected. H_2SO_4 is a common chemical contaminant in the manufacture, storage, transportation and use of AN [6,23]. According to the C80 micro calorimetric studies conducted by Sun et al. [23], H_2SO_4 catalyzes the thermal decomposition of AN by greatly reducing the initial temperature. CuO is an important phase stabilization source for AN. Several studies [6,24–26] have investigated the influence of CuO on thermal decomposition related hazards of AN through micro calorimeter techniques. However, the pyrolysis behaviors when AN was mixed with either CuO or H_2SO_4 have not been studied, which are necessary for the safe use of AN in industry. This study aims to explore the pyrolysis behavior of AN under different radiant fluxes, and the effects of additives on pyrolysis behavior of AN. Findings of this study will provide useful insights for the optimal use of AN as important sustainable energy resources, and will also contribute to the development of appropriate fire detection and firefighting technologies to effectively ensure the safety application of AN and mixtures in industries of interest. 2. Material and experiments Three materials are applied in this study. The pure AN ($>99\%$) was purchased from Beijing Lantai Chemical Technology co., Ltd. The AR grade CuO was purchased from Aladdin (Shanghai) co., Ltd. The AR grade concentrated H_2SO_4 was purchased from Sinopharm Chemical Reagent co., Ltd. Due to the hygroscopicity of AN, mechanical lapping was applied to polish the crystal of AN. The grinded AN samples with uniform particle sizes were placed in a vacuum drying chamber at 55 °C for 24 h to eliminate the potential interference of moisture. The AR grade CuO samples were sealed and stored in confined place to keep dry. The thermal radiation experiments were performed through a DCHA, as shown in Fig. 1(a). It consists of a cone heater, a radiation controller with a temperature panel, an electronic balance, a stainless sample holder, a camera, a computer and an exhaust fume collecting hood with connection to the ventilation system. The cone heater and radiation controller were provided by Suzhou Yangyi Vouch Testing Technology Company, China. The cone heater was built in accordance to the ISO 5660.1 [27,28], which has been applied by fire safety scientists to study the pyrolysis of biomass [29–31], polymers [32,33] and construction materials [27,34–36] for many years. DCHA allows to set radiation heating scenarios with heat flux of $0\sim100$ kW m^{-2} via the radiation controller. The electricity requirement for the radiation controller is 220 V (alternating voltage), 6 KVA with electric leakage. Two pieces of fan-shaped thermal baffle made by asbestos were placed at the bottom of the cone heater during pre-heating to isolate samples from radiation. Pyrolysis experiments started after the temperature (heat flow) was kept stable for 3 min. A Mettler Toledo XP10002S electronic balance with data acquisition of 0.01 g was applied to measure the mass loss of samples under

thermal radiation. The experiments were recorded with a camera and connected to a computer for real-time observation. Note that the measurement of MLR through DCHA is consistent with Cone Calorimeter, but the cost of DCHA is much lower (about 1700 $ for both cone heater and the radiation controller). The sample holder of AN was set as a cuboid with dimension of 60×60 mm to create a two-dimensional heating scenario [27,37]. AN with mass of 30, 50 and 80 g were horizontally spread on the sample holder and heated under certain radiation flux. The sample holder was heightadjustable to ensure that the distance from materials' top surface to the bottom of radiation heater was kept constant. Three typical radiant fluxes in fire (25, 35 and 50 kW m− 2) were selected for experiments [37]. The corresponding temperatures of the radiation controller were around 660 °C, 735 °C and 820 °C, respectively with an error of 2 K. The experimental procedure is presented with a flowchart of Fig. 1(b). Please note that the DCHA also allows the ignition of materials through a 10 kV ignition needle and the radiation controller, which was not emphasized in the current study. In addition to the DCHA, this study also applied an automatic sample grinding machine to mechanically mix AN and CuO (using ceramic beads at frequency of 15 HZ for 90 s), as well as a GeminiSEM 500 to capture the micro surface of AN/CuO mixture.

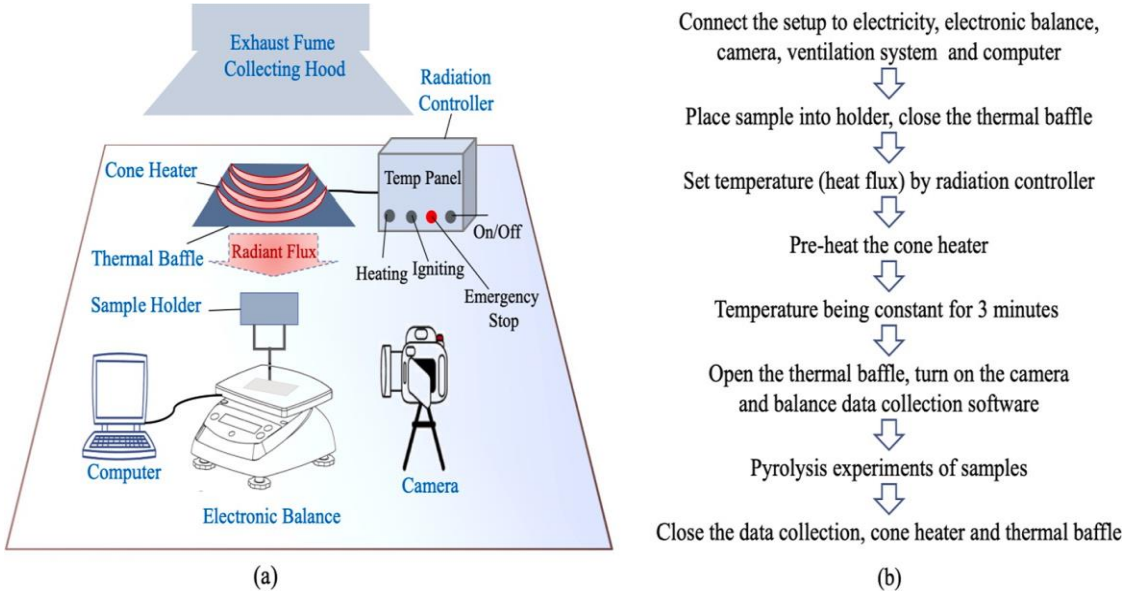

Fig. 1. (a) A schematic diagram of the Desktop Cone Heating Apparatus (DCHA) ; (b) A flowchart of the experimental procedure applied in this study.

Table 1 summarizes the sample information and corresponding radiant fluxes of 18 sets of experiments conducted in this study. Please note that the order of number in the first column is consistent with the order of sample information, e.g. No.2 referring to the experiment with 50 g AN. Before each test, the mixtures containing 6 wt% H_2SO_4 were made by adding 2 mL of liquid into dried AN (30 g) and slowly stirred in an incubator; the AN-CuO samples were manually mixed in a sealed glass bottle using dried AN and certain amount of dried CuO. Since the samples were in shape of crystal particles, it was assumed that the involvement of either CuO or H_2SO_4 would not change the thickness of the sample. Each experiment was duplicated twice to ensure the repeatability. The uncertainty and error of this study has two major sources, the digital instruments of DCHA and the uncertainty propagation in calculations. For the errors in digital instruments, the cone heater delivers an error of 10 % according to the Cone Calorimeter which applies the same cone heater [38]. The balance has a readability of 0.01 g with capacity of 10,100 g, and thus the error of balance can be ignored with sample mass of 30 g, 50 g and 80 g. The calculation

uncertainty is mainly caused by the smoothing of MLR with Stavitzky-Golay method, which will be introduced in Section 3. 3. Results and analysis 3.1. Pyrolysis behavior of pure AN under thermal radiation Numerous thermal decomposition experiments have been conducted using pure AN [1,7]. Despite the variety in applied apparatus and heating procedures, the mass loss always has a single stage when the sample with limited size were uniformly heated during the entire decomposition process. However, the pyrolysis behavior of AN under thermal radiation experiments was found to be different. In the current study, nine sets of experiments (1 ~ 3, 7 ~ 9 and 13 ~ 15) were con- ducted using pure AN under three radiant fluxes.

Table 1

Summary of the sample information and radiant flux.

No.	AN (g)	CuO (wt.%)	H_2SO_4 (wt.%)	Radiant Flux (kW m^{-2})
1, 2, 3	30, 50, 80	0	0	25
4, 5	30	5, 10	0	25
6	30	0	6	25
7, 8, 9	30, 50, 80	0	0	35
10, 11	30	5, 10	0	35
12	30	0	6	35
13, 14, 15	30, 50, 80	0	0	50
16, 17	30	5, 10	0	50
18	30	0	6	50

As an example, Fig. 2 (a) presents the mass loss (the black blocks) and *MLR* (the black line curve) profiles of 80 g AN under 50 kW m—2, corresponding to experi-ment No.15. The *MLR* in unit of g s—1 was calculated as the first-order derivative of time and then smoothed by the Stavitzky-Golay method (the red point curve) [39]. According to the camera, once exposed to radiation, AN started to lose mass and was completely decomposed before 500 s. The entire decomposition process released a lot of smoke, and no flame was observed. From the smoothed *MLR*, the pyrolysis process of AN consisted of four regimes, noted as stage I∼IV in Fig. 2 (a). This is different from the evolution of mass loss stage in TG [7], indicating the complicated heat and mass transfer mechanism when AN in certain thickness was exposed to radiation. From 0 s to 116 s, the *MLR* of AN gradually increased, corresponding to the stage I. Then the value of *MLR* did not change much for about 120 s, referring to the stage II. In these two stages, AN melted and decomposed slowly, noted as the slow decomposition period. The melting behavior was not clearly reflected by either mass or *MLR*, because the pyrolysis process was very fast. Then *MLR* started to in- crease rapidly in the stage III, and reached the MLR_{max} with total sample mass reduced from 80 g to about 30 g. This corresponds to the fast decomposition period. Finally, *MLR* reduced to zero before 600 s and AN was fully decomposed, corresponding to the stage IV, i.e. the decay period.

The aforementioned data processing methodology was applied to all sets of experiments. The results are presented in Fig. 3. The same four- stage evolution characteristic was identified among all samples. An exception was that the values of MLR_{II} were slightly larger than that of MLR_{I} for No. 3, 8, 9, and 15. This is probably due to the complicated heat and mass transfer inside materials with larger sample mass. Overall, the increase rates of *MLR*s in stage II were much slower than that in stage I and III. Despite the differences in sample mass and radiant flux, the *MLR* evolution of AN during pyrolysis consisted of four stages, in which the *MLR* was slowly increasing (stage I), being steady (stage II), rapidly increasing to MLR_{max} (stage III) and reducing

to zero (stage IV), respectively. In stage I and II, AN decomposed relatively slow, noted as the slow decomposition period. Stage III and IV referred to the fast decomposition period and decay period, respectively.

In order to quantitatively characterize the pyrolysis process, seven parameters are defined in this paper, as marked in Fig. 2. The terms of t_{I}, t_{II}, t_{max} and t_{end} (s) refer to the time at the end of stage I, II, III and IV, respectively. The terms of MLR_{I}, MLR_{II} and MLR_{max} (g s—1) refer to the value of *MLR* corresponding to the end of stage I, II and III, respectively. The seven parameters of pure AN are listed in Table 2, in accordance to

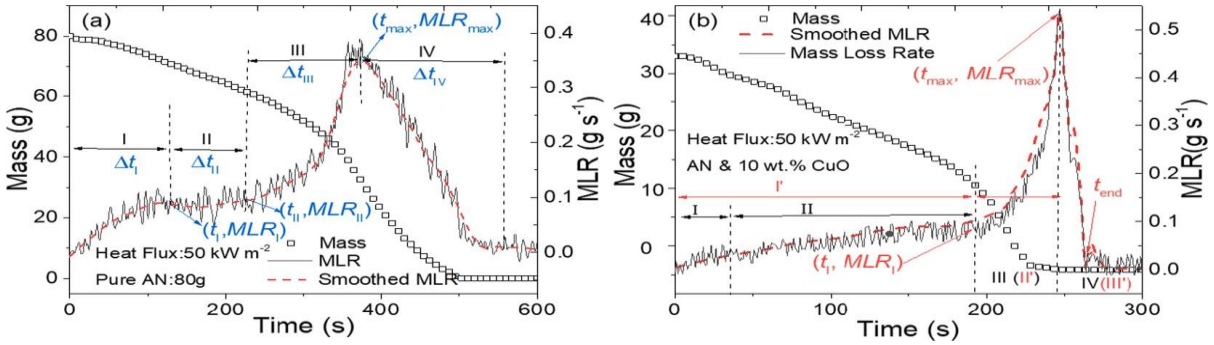

Fig. 2. The pyrolysis stages (I ~ IV) of (a) pure AN, and (b) AN mixed with 10 wt% CuO under radiant flux of 50 kW m—2.

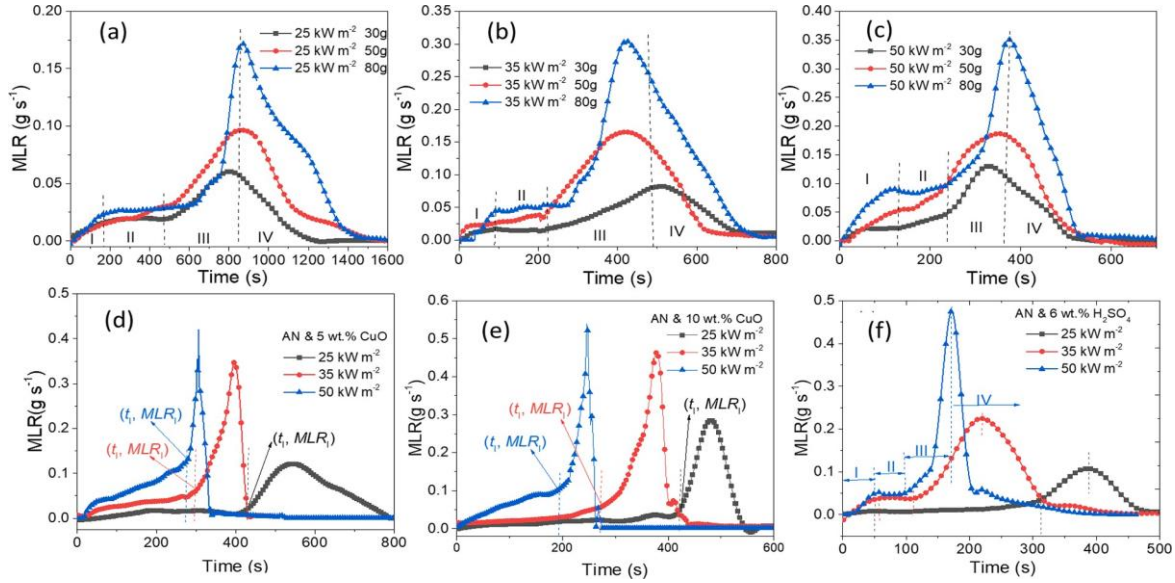

Fig. 3. The pyrolysis stages of, AN under radiant flux of (a) 25 kW m—2, (b) 35 kW m—2 and (c) 50 kW m—2; and AN mixed with (d) 5 wt% CuO, (e) 10 wt% CuO and (f) 6 wt% H_2SO_4 under three radiant fluxes. No. 1～3, 7～9 and 13～15, respectively. The order of number is consistent with the experimental information listed in Table 1. These parameters quantitatively indicate how the pyrolysis process of AN was evolved with change of sample mass, radiant flux and radiation time. Please note that the *MLR* data in Table 2 are limited to two decimal places because the readability of balance is 0.01 g. The experimental uncertainties of *MLR* are computed as two standard deviations of the mean.

It can be seen from Table 2 that, under a certain radiant flux, the t_{max} values of samples in different masses were close to each other, indicating the reliability of the experiment. The time corresponding to each decomposition stage is roughly described by a time region as follows. When

AN was exposed to radiant flux of 25 kW m—2, the time period of stage I (t_I), II (t_I～t_{II}), III (t_{II}～t_{max}) and IV (t_{max}～t_{end}) was in the region of 0～200 s, 200～500 s, 500～900 s and 900～1500 s, respectively; the t_{max} was at about 800～900 s. Similarly, when AN was exposed to radiant flux of 35 kW m—2, the time of stage I, II, III and IV was in the region of 0～100 s, 100～230 s, 230～500 s and 500～800 s, respec- tively; the t_{max} was in the region of 400～500 s. At 50 kW m—2, the time of four pyrolysis stages was in 0～120 s, 120～240 s, 240～380 s and 380～600 s, respectively; and the t_{max} was in the region of 300～400 s.

Besides, a larger sample mass led to higher MLR_{max}. For example, with mass increasing from 30 g to 80 g, the MLR_{max} increased by nearly 2.7 times at 35 kW m—2. This indicated that a larger accumulation mass mainly acted on the fast decomposition period, i.e. the stage III.

For the effects of radiant flux, it is obvious that a larger radiant flux could accelerate the entire pyrolysis process by reducing the time of each stage and increasing the t_{max}. Taking the case with 80 g AN as an example, when the radiant flux was increased from 25 kW m—2 (No. 3) to 50 kW m—2 (No. 15), the t_{max} increased twice (500 s), the MLR_{max} reduced by over a half; and the value of t_{end} was also reduced by over a half (900 s). The same change fashion was observed for the cases with mass of 30 g and 50 g. Since the time region of pyrolysis stages was directly linked to radiant flux, the statistical data from Table 2 could be used as reference data for emergency response planning when pure AN is exposed to external fire. For example, if the thermal radiation of external fire was expected to be about 50 kW m—2, effective firefighting strategies such as cooling and thermal insulation should be adopted before 380 s to prevent AN from rapid decomposition. Detailed discussions about this topic are available in Section 3.4.

Table 2

Summary of the quantitative characterization parameters of all tests.

No.	t_I (s)	MLR_I (g s^{-1})	t_{II} (s)	MLR_{II} (g s^{-1})	t_{max} (s)	MLR_{max} (g s^{-1})	t_{end} (s)
1	247	0.02 ± 4.6%	472	0.02 ± 2.3%	804	0.06 ± 6.9%	1300
2	270	0.02 ± 3.9%	310	0.02 ± 2.3%	864	0.10 ± 8.1%	1500
3	257	0.03 ± 5.2%	620	0.03 ± 3.0%	874	0.17 5.0%	1500
4	400	0.01 ±	N/A	N/A	548	0.12 4.1%	800
5	394	0.03 ± 4.2%	N/A	N/A	482	0.29 ± 8.4%	600
6	51	0.01 ± 1.0%	130	0.01 6.2%	374	0.11 6.6%	500
7	90	0.02 ± 2.2%	223	0.02 ± 1.5%	505	0.08 4.9%	1100
8	45	0.02 ± 5.3%	215	0.04 ± 4.0%	424	0.17 ± 3.0%	1100
9	96	0.05 ± 4.2%	279	0.06 ±	422	0.30 3.7%	900
10	270	0.05 ± 2.9%	N/A	N/A	397	0.35 ± 6.8%	500
11	277	0.05 ± 2.3%	N/A	N/A	380	0.46 3.6%	500
12	60	0.04 ± 4.5%	118	0.04	220	0.23 5.1%	400
13	58	0.02 ± 2.0%	117	0.02 ± 3.2%	335	0.13 ± 2.5%	600
14	137	0.06 ± 4.6%	167	0.06 ± 2.9%	357	0.19 8.3%	700
15	116	0.09 ± 3.5%	236	0.10 ±	373	0.35 5.8%	600
16	278	0.13 ± 2.1%	N/A	N/A	307	0.42 ± 6.8%	400
17	178	0.09 ± 3.5%	N/A	N/A	246	0.54 4.9%	300
18	56	0.05 ±	100	0.05	172	0.48 3.8%	300

3.2. Pyrolysis behavior of AN mixtures under thermal radiation

Two typical additives were added to AN to explore their effects on the pyrolysis behavior of AN. The effect of CuO was studied by adding 5 wt% and 10 wt% CuO to AN and exposing the mixtures to radiant flux of 25 kW m—2, 35 kW m—2 and 50 kW m—2, respectively. The same data processing methodology mentioned in Section 3.1 was applied for analysis. The results are shown in Fig. 2 (b). Since CuO did not partic- ipate in the mass loss process due to the catalytic effects [6,24–26], the original mass of CuO was subtracted from the total mass of mixture before processing the data. Similar to pure AN, once exposed to thermal radiation, the AN/CuO mixtures started to loss mass for about 250 s till all of the AN samples were decomposed into gases. A large amount of gas was released during the whole pyrolysis process, and no flame was observed.

Comparing to the *MLR* profile in Fig. 2 (a), the major difference in Fig. 2 (b) is that the aforementioned four-stage evolution characteristic was reduced into three stages. This is also different from the mass loss process of AN/CuO observed by TG experiments. In the slow decomposition period, the *MLR* continuously increased with a steady increase rate and finally reached $MLR_{I/II}$ of 0.09(3.5%) g s—1 at 178 s. Then in the fast decomposition period, the increase rate of *MLR* became larger; *MLR* quickly reached the MLR_{max} of 0.54(4.9%) g s—1 at 246 s, and then reduced to 0 before 300 s. The detailed time and *MLR* values of each stage are summarized in Table 2 (No. 17). Comparing to pure AN with the same mass under the same radiant flux (No.13), the t_{max} was reduced by one third, the total pyrolysis time was 50% shorter, and the MLR_{max} increased by four times. This indicates that the involvement of CuO could accelerate the entire pyrolysis process by merging the first two slow decomposition stages and significantly enhancing the reaction rate in the fast decomposition period. The same three-stage evolution char-

acteristic of *MLR*s was observed among AN/CuO mixtures with other mass proportions under other radiant fluxes, as shown in Fig. 3 (d) ~ (e). The boundaries of stage I and II for each curve were marked with a dash line. The detailed values of t_I, MLR_I, t_{max}, MLR_{max} and t_{end} are all listed in Table 2, corresponding to No. 4 ~ 5, 10 ~ 11 and 16 ~ 17.

From Fig. 3 and Table 2, the catalytic effects of CuO depended on both mass proportion in the mixture and the external radiant flux. Firstly, the larger the mass proportion, the shorter time required by AN to reach a higher MLR_{max}. For example, when proportion of CuO was third, the t_{end} reduced by a quarter, and the MLR_{max} increased with a sharper peak in profile. Secondly, the effects of thermal radiation were primarily presented by the time reduction in each pyrolysis stage, as well as the increase of MLR_{max}. In Fig. 3 (d), both t_{max} and t_{end} reduced approximately half when radiant flux was increased from 25 to 50 kW m—2, while the MLR_{max} increased by nearly 2.5 times. The same fashion was shown in Fig. 3 (e) where the *MLR* profile became much sharper under a higher radiant flux, indicating the dramatic catalytic effects of CuO on pyrolysis of AN. The effects of H_2SO_4 on pyrolysis of AN were studied by adding 2 mL concentrated H_2SO_4 to AN and exposing the mixtures to three radiant fluxes. Similarly, mass of the AN/H_2SO_4 mixture started to reduce continuously once the experiments started, as presented in Fig. 3 (f). The pyrolysis process ended before 500 s, 400 s and 300 s under 25 kW m—2,35 kW m—2 and 50 kW m—2, respectively. Different from AN/CuO mixtures which had certain amount of final residue (the unreacted CuO), both AN and H_2SO_4 were fully decomposed into gases. Besides, the entire pyrolysis process released a large amount of smoke and no flame was observed.

The same data processing methodology was applied to handle the mass loss data of AN/H_2SO_4 mixtures. Same as the four pyrolysis stages of pure AN, the evaluation of *MLR*s also consisted of four stages in which the mixture increased slowly, being stable, increased rapidly and decreased to zero. The values of t_I, MLR_I, t_{II}, MLR_{II}, t_{max}, MLR_{max} and t_{end} are summarized in Table 2, corresponding to No. 6, 12 and 18, respec- tively. Comparing to pure AN with the same mass (No. 1, 7 and 13), the involvement of H_2SO_4 did not change the pyrolysis stages, but signifi- cantly accelerated the decomposition rates. In other words, H_2SO_4

participated in the pyrolysis by chemical decomposition reactions and was fully decomposed. Under radiant flux of 25 kW m—2, the involve- ment of H_2SO_4 reduced both t_{max} and t_{end} by more than 50%, and doubled the MLR_{max}. The same fashion was shown with the cases under other two radiant fluxes. For the effects of radiation, the *MLR* profile at 50 kW m—2 showed a much sharper peak, and t_{max} was 200 s earlier than that of 25 kW m—2. Comparing Fig. 3 (d)~(e) to Fig. 3 (f), although both CuO and H_2SO_4 significantly accelerated the pyrolysis of AN, the *MLR* profiles were in different shapes, especially under the condition of high radiant fluxes. The *MLR* profiles of AN/H_2SO_4 were in a shape of a narrow symmetry gauss curve, similar to the profiles of pure AN in Fig. 2. However, the *MLR* curves in Fig. 3 (f) were in a dissymmetric shape with much sharper *MLR* peaks. Since the *MLR* evolution profiles were determined by the pyrolysis reaction mechanism of samples, these curve shapes also indicated the different catalytic effects of CuO and H_2SO_4 on the pyrolysis of AN. Further analyses of their mechanisms are presented in Section 3.3.

3.3 Pyrolysis structure and mechanism analysis

The four-stage evolution characteristic of MLRs was caused by both temperature and mass concentration gradients inside the samples, which could be very complicated. Izato et al. 40] proposed a qualitative combustion wave structure model for AN mixed with carbon. Their model

was adapted in this paper to explain the pyrolysis behavior of AN under thermal radiation scenario. When exposed to radiation, the entire AN samples could be qualitatively divided into four zones according to the spatial positions, dominating physical states and chemical reactions, as shown in Fig. 4 (a). The first zone on the sample bottom refers to the unreacted samples. Above zone 1 is the second zone where the dominating behavior of samples include melting, thermal decomposition and gas evolution. Most of the samples in zone 1 and zone 2 are of condensed phase (liquid or solid). The third zone above zone 2 corresponds to the preheating and diffusion of generated gases. And the zone 4 is mainly related to the combustion and evolution of gases. Please note that this model presents a simplified illustration with assumption that, only the dominating state of sample component and major thermal behavior could determine the physical and chemical interactions among the four zones. In real fire scenario, zone 2 may also consist of gaseous components as they were continuously generated during thermal decomposition.

For samples with certain thickness, the evolution of reaction zones in the pyrolysis structure model was related to the primary thermal decomposition reactions in the condensed phases [40]. Previous re- searchers [1,8,41] have widely accepted that, the decomposition of AN could be explained by two kinds of mechanisms, the ionic reactions (with sample at 200～300 ◦C, low reaction rate) and radical reactions (with sample above 290 ◦C, high reaction rate). Since the temperature of AN surface under radiation was in the range of 200～500 oC [42,43], both ion reactions and radical reactions occurred in the reaction zones. The evolution of pyrolysis stages and corresponding decomposition pathways are as follows.

First, when AN was exposed to radiation, the thermal decomposition zone was created, in which AN on the top layer melted through R1 at about 170 ◦C [42,43]. The liquids continuously decomposed through ionic R2. Although this reaction was endothermic, the radiation from cone heater continuously provided energy and supported the further reactions of NH_3 and HNO_3 through R3～R6 [40,41,44].

Among these reactions, acidic species such as ammonium ion, hydronium ion and nitric acid drastically increased the decomposition rate of AN, while some bases such as ammonia or water retarded the decomposition.

CONCLUSIONS

The uncontrolled external fire has been proved by literatures to be the primary cause of dramatic explosion accidents of ammonium nitrate in industry, but limited studies have been conducted to investigate the behavior of ammonium nitrate in fire. By simulating typical fire sce- narios, this paper conducted a series of thermal radiation experiments through an ISO 5660 cone heater to explore the pyrolysis behavior of ammonium nitrate, ammonium nitrate/copper oxide and ammonium nitrate/sulfuric acid. Through in-depth analysis of the mass loss, a four- stage characteristic process (from stage I to stage IV) in accordance to three dominating pyrolysis periods (slow decomposition, fast decom- position and decay) was identified. Data of both mass loss rate and time at each stage were collected. The increase of accumulation mass did not significantly change the stage transition time, and yet higher radiant flux mainly accelerated the reaction rate in fast decomposition period. Four pyrolysis structure models were established to relate the combustion behavior at different pyrolysis stages. Besides, it was found that the involvement of copper oxide and sulfuric acid accelerated the pyrolysis rate of ammonium nitrate through different catalytic mechanisms. Sul- furic acid did not change the four-stage characteristic

process, but enhanced the decomposition reaction rate of each stage by generating more nitric acid. Copper oxide catalyzed the pyrolysis of ammonium nitrate by merging the stage I and II and generating a sharp and un- symmetrical mass loss rate profile in the fast decomposition period. Five burning timelines were developed to qualitatively describe the pyrolysis behavior of ammonium nitrate under different scenarios. The safety time for fire safety control depended on both radiant flux and sample compositions. An emergency response time of 75 s is recommended to isolate materials from external fire, if samples including pure ammo- nium nitrate, ammonium nitrate mixed with 10 wt% copper oxide or less, and ammonium nitrate contaminated by 6 wt% sulfuric acid or less are exposed to external fire with radiant flux of 50 kW m—2 at most.

REFERENCES

1. V. Babrauskas, D. Leggett, Thermal decomposition of ammonium nitrate, Fire Mater. 44 (2020) 250–268. https://doi:10.1002/fam.2797.
2. X. Baraza, A. Pey, J. Gim´enez, The self-sustaining decomposition of ammonium nitrate fertiliser: Case study, Escombreras valley, Spain, J. Hazard. Mater. 387 (2020), 121674, https://doi.org/10.1016/j.jhazmat.2019.121674.
3. J. Jos, S. Mathew, Ammonium Nitrate as an Eco-Friendly Oxidizer for Composite Solid Propellants: Promises and Challenges, Crit. Rev. Solid State Mater. Sci. 42 (2017) 470–498. https://doi:10.1080/10408436.2016.1244642.
4. C. Oommen, S.R. Jain, Ammonium nitrate: a promising rocket propellant oxidizer, J. Hazard. Mater. 67 (1999) 253–281, https://doi.org/10.1016/S0304-3894(99) 00039-4.
5. G. Marlair, M.-A.A. Kordek, Safety and security issues relating to low capacity storage of AN-based fertilizers, J. Hazard. Mater. 123 (2005) 13–28. https://doi: 10.1016/j.jhazmat.2005.03.028.
6. S. Chaturvedi, P.N. Dave, Review on Thermal Decomposition of Ammonium Nitrate, J. Energ. Mater. 31 (2013) 1–26. https://doi:10.1080/07370652.20 11.573523.
7. M. Yang, X. Chen, Y. Wang, B. Yuan, Y. Niu, Y. Zhang, R. Liao, Z. Zhang, Comparative evaluation of thermal decomposition behavior and thermal stability of powdered ammonium nitrate under different atmosphere conditions, J. Hazard. Mater. 337 (2017) 10–19. https://doi:10.1016/j. jhazmat.2017.04.063.
8. J.C. Oxley, J.L. Smith, E. Rogers, M. Yu, Ammonium nitrate: thermal stability and explosivity modifiers, Thermochim. Acta. 384 (2002) 23–45, https://doi.org/ 10.1016/S0040-6031(01)00775-4.
9. R. Gunawan, D. Zhang, Thermal stability and kinetics of decomposition of ammonium nitrate in the presence of pyrite, J. Hazard. Mater. 165 (2009) 751–758. https://doi:10.1016/j. jhazmat.2008.10.054.
10. K. Fujisato, H. Habu, A. Miyake, K. Hori, Thermal decomposition of ammonium nitrate modeling of thermal dissociation in thermal analysis, Sci Technol Energ Mater. 75 (2014) 28–36, https://doi.org/10.1016/j.jhazmat.2017.04.063.
11. V. P. Sinditskii, V.Y. Egorshev, A.I. Levshenkov, V. V. Serushkin, Ammonium nitrate: Combustion mechanism and the role of additives, in: Propellants, Explos. Pyrotech., John Wiley & Sons, Ltd, 2005: pp. 269–280. https://doi:10.1002/ prep.200500017.

12. Z. Han, S. Sachdeva, M.I. Papadaki, M.S. Mannan, Ammonium nitrate thermal decomposition with additives, J. Loss Prev. Process Ind. 35 (2015) 307–315. https://doi:10.1016/J.JLP.2014.10.011.
13. H.Q. Cao, Q.L. Duan, H. Chai, X.X. Li, J.H. Sun, Experimental study of the effect of typical halides on pyrolysis of ammonium nitrate using model reconstruction, J. Hazard. Mater. 384 (2020), 121297, https://doi.org/10.1016/j. jhazmat.2019.121297.
14. H.Q. Cao, L. Jiang, Q.L. Duan, D. Zhang, H.D. Chen, J.H. Sun, An experimental and theoretical study of optimized selection and model reconstruction for ammonium nitrate pyrolysis, J. Hazard. Mater. 364 (2019) 539–547, https://doi.org/10.1016/ j.jhazmat.2018.10.048.
15. V. Babrauskas, Explosions of ammonium nitrate fertilizer in storage or transportation are preventable accidents, J. Hazard. Mater. 304 (2016) 134–149. https://doi:10.1016/j.jhazmat.2015.10.040.
16. Q. Chen, M. Wood, J. Zhao, Case study of the Tianjin accident: Application of barrier and systems analysis to understand challenges to industry loss prevention in emerging economies, Process Saf. Environ. Prot. 131 (2019) 178–188, https://doi. org/10.1016/j.psep.2019.08.028.
17. F. Gui, J. Wang, M. Yan, G. Fu, J. Wang, M. Yan, F. Gui, J. Wang, M. Yan, G. Fu, J. Wang, M. Yan, Anatomy of Tianjin Port fire and explosion: Process and causes, Process Saf. Prog. 35 (2016) 216–220. https://doi:10.1002/prs.11837.
18. L. Ding, J. Ji, F. Khan, Combining uncertainty reasoning and deterministic modeling for risk analysis of fire-induced domino effects, Saf. Sci. 129 (2020), 104802, https://doi.org/10.1016/j.ssci.2020.104802.
19. J. Ji, Q. Tong, F. Khan, M. Dadashzadeh, R. Abbassi, Risk-Based Domino Effect Analysis for Fire and Explosion Accidents Considering Uncertainty in Processing Facilities, Ind. Eng. Chem. Res. 57 (2018) 3990–4006. doi:10.1021/acs. iecr.8b00103.
20. L. Ding, F. Khan, J. Ji, A novel approach for domino effects modeling and risk analysis based on synergistic effect and accident evidence, Reliab. Eng. Syst. Saf. 203 (2020), 107109, https://doi.org/10.1016/j.ress.2020.107109.
21. Q. Sun, L. Jiang, M. Li, J. Sun, Assessment on thermal hazards of reactive chemicals in industry: State of the Art and perspectives, Prog. Energy Combust. Sci. 78 (2020), 100832, https://doi.org/10.1016/j.pecs.2020.100832.
22. Z. Han, H.J. Pasman, M.S. Mannan, Extinguishing fires involving ammonium nitrate stock with water: Possible complications, J. Fire Sci. 35 (2017) 457–483, https://doi.org/10.1177/0734904117735264.
23. J. Sun, Z. Sun, Q. Wang, H. Ding, T. Wang, C. Jiang, Catalytic effects of inorganic acids on the decomposition of ammonium nitrate, J. Hazard. Mater. 127 (2005) 204–210. https://doi:10.1016/j.jhazmat.2005.07.028.
24. Z. Xu, G. Xu, X. Fu, Q. Wang, The mechanism of nano-CuO and CuFe2o4 catalyzed thermal decomposition of ammonium nitrate, Nanomater. Nanotechnol. 6 (2016) 184798041668169. https://doi:10.1177/1847980416681699.
25. A.A. Vargeese, K. Muralidharan, Kinetics and mechanism of hydrothermally prepared copper oxide nanorod catalyzed decomposition of ammonium nitrate, Appl. Catal. A Gen. 447–448 (2012) 171–177, https://doi.org/10.1016/j. apcata.2012.09.027.

26. K. Kajiyama, Y. Izato, A. Miyake, Thermal characteristics of ammonium nitrate, carbon, and copper(II) oxide mixtures, J. Therm. Anal. Calorim. 113 (2013) 1475–1480. https://doi:10.1007/s10973-013-3201-5.
27. B. Schartel, M. Bartholmai, U. Knoll, Some comments on the use of cone calorimeter data, Polym. Degrad. Stab. 88 (2005) 540–547, https://doi.org/ 10.1016/j.polymdegradstab.2004.12.016.
28. I.S.O. 5660-1, Reaction-to-fire tests-Heat release, smoke production and mass loss rate-Part 1: heat release rate (cone calorimeter method), Geneva, Switz. Int. Stand. Organ. (2002).
29. H.S. Ding, H. Jiang, Self-heating co-pyrolysis of excessive activated sludge with waste biomass: Energy balance and sludge reduction, Bioresour. Technol. 133 (2013) 16–22. https://doi:10.1016/j.biortech.2013.01.090.
30. R. Emberley, T. Do, J. Yim, J.L. Torero, Critical heat flux and mass loss rate for extinction of flaming combustion of timber, Fire Saf. J. 91 (2017) 252–258, https://doi.org/10.1016/j.firesaf.2017.03.008.
31. O. Grexa, H. Lübke, Flammability parameters of wood tested on a cone calorimeter, Polym. Degrad. Stab. 74 (2001) 427–432, https://doi.org/10.1016/S0141-3910 (01)00181-1.
32. Y. Ding, S.I. Stoliarov, R.H. Kraemer, Pyrolysis model development for a polymeric material containing multiple flame retardants: Relationship between heat release rate and material composition, Combust. Flame. 202 (2019) 43–57, https://doi. org/10.1016/j.combustflame.2019.01.003.
33. M.B. McKinnon, Y. Ding, S.I. Stoliarov, S. Crowley, R.E. Lyon, Pyrolysis model for a carbon fiber/epoxy structural aerospace composite, J. Fire Sci. 35 (2017) 36–61. https://doi:10.1177/0734904116679422.
34. B.T. Rhodes, J.G. Quintiere, Burning rate and flame heat flux for PMMA in a cone calorimeter, Fire Saf. J. 26 (1996) 221–240, https://doi.org/10.1016/S0379-7112 (96)00025-2.
35. B. Li, A study of thermal degradation and decomposition of rigid poly (vinyl chloride) with metal oxides using thermogravimetry and cone calorimetry, Polym. Degrad. Stab. 68 (2000) 197–204, https://doi.org/10.1016/S0141-3910(00) 00002-1.
36. J. Luche, T. Rogaume, F. Richard, E. Guillaume, Characterization of thermal properties and analysis of combustion behavior of PMMA in a cone calorimeter, Fire Saf. J. 46 (2011) 451–461, https://doi.org/10.1016/j.firesaf.2011.07.005.
37. V. Babrauskas, The cone calorimeter, in: SFPE Handb. Fire Prot. Eng., Springer, 2016: pp. 952–980.
38. G. Wypych, Testing Methods in Filled Systems, in: Handbook of Fillers (Fourth Edition), Elsevier, 2016: pp. 627–664. doi:10.1016/B978-1-895198-91-1.50016-6.
39. J.E.J. Staggs, Savitzky-Golay smoothing and numerical differentiation of cone calorimeter mass data, Fire Saf. J. 40 (2005) 493–505, https://doi.org/10.1016/j. firesaf.2005.05.002.
40. Y.I. Izato, A. Miyake, S. Date, Combustion characteristics of ammonium nitrate and carbon mixtures based on a thermal decomposition mechanism, Propellants, Explos. Pyrotech. 38 (2013) 129–135. https://doi:10.1002/prep.201100106.
41. K.R. Brower, J.C. Oxley, M. Tewari, Evidence for homolytic decomposition of ammonium nitrate at high temperature, J. Phys. Chem. 93 (1989) 4029–4033, https://doi.org/10.1021/j100347a033.

42. A. Miyake, Y. Izato, Thermal Decomposition Behaviors of Ammonium Nitrate and Carbon Mixtures, Int. J. Energ. Mater. Chem. Propuls. 9 (2010) 523–531. https:
43. //doi:10.1615/IntJEnergeticMaterialsChemProp.2011001429.
44. Y. Wada, K. Hori, M. Arai, Combustion mechanism of mixtures of guanidine nitrate, ammonium nitrate, and basic copper nitrate, Sci Technol Energ Mater. 71 (2010) 83–87.
45. Y. Izato, A. Miyake, Thermal decomposition of molten ammonium nitrate (AN), J. Therm. Anal. Calorim. 122 (2015) 595–600. https://doi:10.1007/s10973-0 15-476